Bioorganic Chemistry 92 (2019) 103193

Contents lists available at ScienceDirect

Bioorganic Chemistry

journal homepage: www.elsevier.com/locate/bioorg

Synthesis, biological activity and molecular modeling of a new series of condensed 1,2,4-triazoles

Youness El Bakri[a,b,*], Ilias Marmouzi[c], Meryem El Jemli[c], El Hassane Anouar[d,*], Subramani Karthikeyan[b,*], Abdallah Harmaoui[a], My El Abbes Faouzi[c], Joel T. Mague[e], El Mokhtar Essassi[a]

[a] Laboratoire de Chimie Organique Hétérocyclique, Centre de Recherche des Sciences des Médicaments, Pôle de Compétences Pharmacochimie, URAC 21, Faculté des Sciences, Université Mohammed V Rabat, Avenue Ibn Battouta, BP 10014 Rabat, Morocco
[b] Organic Chemistry Department, Science Faculty, RUDN University Miklukho-Maklaya st. 6, 117198 Moscow, Russian Federation
[c] University Mohammed V in Rabat, Faculté de Médicine et de Pharmacie, Laboratoire de Pharmacologie et Toxicologie, équipe de Pharmacocinétique, BP 6203, Rabat Instituts, Rabat, Morocco
[d] Department of Chemistry, College of Sciences and Humanities, Prince Sattam bin Abdulaziz University, P.O. Box 83, Al Kharj 11942, Saudi Arabia
[e] Department of Chemistry, Tulane University, New Orleans, LA 70118, USA

ARTICLE INFO

Keywords:
1,2,4-Triazoles
Pyrazolotriazole
Antidiabetic
Antioxidant activity
Docking study
Molecular dynamics
DFT calculations

ABSTRACT

A ring transformation of 6-methyl-7*H*[1,2,4]triazolo [4,3-b][1,2,4] triazepine-8(9*H*)-ones (thiones) in the presence of acetic anhydride give rise to a new series of 17 condensed 1,2,4-triazole derivatives (**1–17**). Plausible mechanisms are proposed and show the formation of a beta fused β-lactam moiety. The compounds were tested for their (i) inhibitory potential on digestive enzymes (*α*-amylase and *α*-glucosidase), and (ii) antioxidant activity using radical scavenging (DPPH and ABTS radicals) and ferric reducing power assays. The compounds showed interesting and promising antidiabetic activities compared to the reference drug Acarbose. Molecular docking study has been carried out to determine the binding mode interactions between these derivatives and the targeted enzymes. The results showed the strength of intermolecular hydrogen bonding in ligand-receptor complexes as an important descriptor in rationalizing the observed inhibition results. Moreover, molecular dynamics simulations are also performed for the best protein-ligand complex to understand the stability of small molecule in a protein environment. To shed light on the antioxidant activity of the synthesized compounds and the mechanism involved in DPPH free radical, DFT calculations were performed at the B3P86/6-311 + + G(d,p) level using the polarizable continuum model. The effect of aprotic solvent on bond dissociation enthalpies (BDEs) is investigated by calculating and comparing BDEs of **1** in methanol and dimethylsulfoxide as solvents using PCM. The obtained results show that the mechanism of action depends on the basic skeleton and the presence of substituted functional groups in these derivatives. BDEs are found to be slightly influenced by the aprotic solvent of less than 0.01 kcal/mol compared with those obtained in methanol.

1. Introduction

Heterocyclic compounds, whether natural or synthetic, demonstrate fascinating biological properties. The subgroup 1,2,4-triazole and their derivatives constitute an important class of heterocyclic compounds with diverse agricultural, industrial and biological properties and applications [1], including anti-microbial [2,3], sedative, anti-convulsant and anti-inflammatory activities [4]. The synthesis of these heterocycles has received considerable attention in recent years [5–8]. Yasemin Ünver et al., synthesized and tested the antioxidant activity of series of new 1,2,4-triazole-1,3,4-oxadiazole, 1,2,4-triazole-triazole/thiol, 1,2,4-triazole-Schiff bases, and 1,2,4-triazole compounds possessing morpholine and Schiff base rings using DPPH• radical scavenging and ferric reducing/antioxidant power methods and the test results showed their good antioxidant activities [9]. A series of eleven 1,2,4-triazolylbenzotriazoles have been synthesized and evaluated for their antioxidantactivities and some of the1,2,4-triazolylbenzotriazoles substitute phenolic group were found to be good antioxidants [10].

Several experimental and theoretical studies of the structure-antioxidant activity relationships of synthesized and natural polyphenols

* Corresponding authors at: Organic Chemistry Department, Science Faculty, RUDN University Miklukho-Maklaya st. 6, 117198 Moscow, Russian Federation (Y. El Bakri).
E-mail addresses: yns.elbakri@gmail.com (Y. El Bakri), anouarelhassane@yahoo.fr (E.H. Anouar), 92karthy@gmail.com (S. Karthikeyan).

https://doi.org/10.1016/j.bioorg.2019.103193
Received 10 May 2019; Received in revised form 10 July 2019; Accepted 10 August 2019
Available online 12 August 2019
0045-2068/

proved that this activity mainly depends on the presence of phenolic hydroxyl groups, and their capacity to donate a hydrogen atom to quench free radicals [7–16]. Density functional theory (DFT) has become a very popular tool to rationalize quantitative structure activity relationship (QSAR), since it successfully describes the hydrogen atom transfer of OH phenolic groups to quench free radicals [11,12].

As part of our program to develop new biologically active compounds [13,14], herein, we report the synthesis of some new condensed 1,2,4-triazole compounds through the action of acetic anhydride on 6-methyl-7*H*[1,2,4]triazolo [4,3-b][1,2,4] triazepin-8(9*H*)-ones (thiones). It is worthy to emphasize that triazolotriazepine derivatives have been used as potent inhibitors of bone resorption [15]. They also exhibit an anti-fungal activity [16]. This work has been performed in view of the potential biological activity of fused azepines [17–19] and as part of our interest in the synthesis of new heterocyclic systems containing triazole and triazepine rings [20–22].

In order to consider the influence of the presence of a β-lactam and a *β*-thiolactam in the seven-membered ring on the course of the reactions described, it seemed interesting to study the reactions involving acetic anhydride and 1,2,4-triazolo [4,3-b][1,2,4]triazepine-2-one and also 1,2,4-triazolo [4,3-b][1,2,4]triazepine-2-thione prepared by sulfurization of 1,2,4-triazolo [4,3-b][1,2,4]triazepin-2-one.

2. Results and discussion

It is well known that the unsaturated seven-membered heterocycles transpose easily to give new five or six-membered heterocycles. This transposition can be carried out essentially according to two mechanisms. The first mechanism involves an opening of the ring followed by intramolecular cyclization of the intermediates obtained. The second one involves a transannular reaction. In both mechanisms, the ring transformation leads to the formation of the most stable compound rather than the initial products, particularly if they have an eight-electron conjugate system and the result is a six-electron aromatic system. Compound **1** reacted with acetic anhydride on heating for 15 min and lead to the formation of two products, **2** and **3** which have pyrazolotriazole and azetopyrazolotriazole structures, respectively (Scheme 1).

The structure of **3** was established on the basis of ^{1}H and ^{13}C NMR spectroscopic data. The ^{1}H NMR spectrum highlights, in particular, the presence of two signals at 2.2 and 2.4 ppm, attributable to the acetyl and methyl groups, respectively, attached to the pyrazole moiety. The downfield signal at 8.9 ppm corresponds to the triazole proton. The ^{13}C NMR spectrum shows the presence of two signals at 161.7 and 171.7 ppm whose correspond to the carbonyl groups of the *β*-lactam and the acetyl group, respectively. The signal at 90.7 ppm is due to the quaternary carbon at position 9 (compound 1) of the tricyclic system.

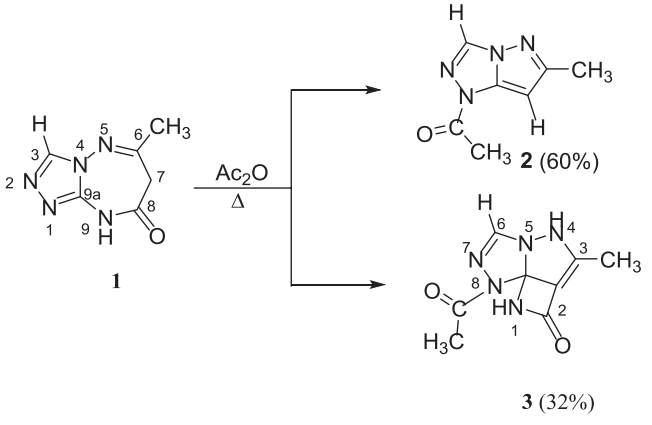

Scheme 1. Synthesis of pyrazolotriazole **(2)** and azetopyrazolotriazole (**3**) derivatives.

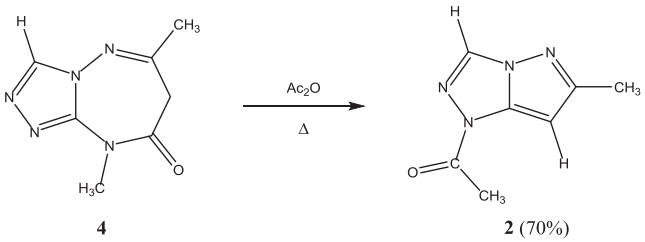

Scheme 2. Transposition of **4** to **2**.

Studying the mechanism of this transposition, we first wanted to know if the hydrogen atom attached to the nitrogen atom in position 9 (compound 1) intervenes in the contraction of the seven-membered ring. For this purpose, we reacted acetic anhydride under the above conditions with the *N*-methylated compound **4** and obtained the same product **2**. This result shows that the elimination of the group −RN−C═O is likely involved in the transposition and that the proton linked to the nitrogen atom at position 9 (compound 1) does not play a fundamental role (Scheme 2):

We have also investigated the roles played by the hydrogen atoms attached to the carbon in position 7 (compound 4) of the bicyclic system in the formation of the products in this rearrangement. Thus, the reaction is carried out on 1,2,4-triazolo [4,3-b][1,2,4]triazepines having mono-or disubstitution at position 7. Halogenation at position 7 leads to the formation of **5–6** triazolotriazepines (Scheme 3).

Thus, the action of acetic anhydride on the compound disubstituted at position 7 leads exclusively to the monoacetylated compound **8**. The structure has been confirmed by ^{1}H NMR spectrum ($DMSOd_{6}$) which shows the presence of a signal at 2.32 ppm attributable to the acetyl group (Scheme 4).

By the reaction of acetic anhydride with compound **6**, which has a hydrogen atom at the 7 position, it has been possible for us to exclusively isolate pyrazolotriazole **9** from rearrangement of the seven-membered ring (Scheme 5).

Similarly, the presence of a hydrogen atom linked to the carbon in position 7 is necessary for the rearrangement of triazolotriazepinones to pyrazolotriazoles. This was also confirmed during the action of hot acetic anhydride on compound **7** dichlorinated at the 7-position. The normally expected compound was isolated (Scheme 6).

Based on these results, we have been able to propose a mechanism to explain the rearrangement of the triazolotriazepine compounds. The mechanism that we envisage postulates that the initial stage of the ring contraction is a diacetylation reaction on the nitrogen atoms N_1 and N_9 which leads to the intermediate **B**. From the latter, the acetate ions attack proton from the methylene group at position 7. The carbanion thus formed can, by a transannular reaction, attack the C_{9a}—N_1 double bond, creating a tricyclic compound **C**. The latter can stabilize in two ways: the first corresponds to the evolution of **C** to a tautomeric form stabilized by resonance to give **3**, it can be inferred that the conjugated tautomer of D is more stable than its unconjugated C tautomer. The second corresponds to the subsequent decomposition with the elimination of cyanic acid derivatives to yield **2** with a pyrazolotriazole structure (Scheme 7).

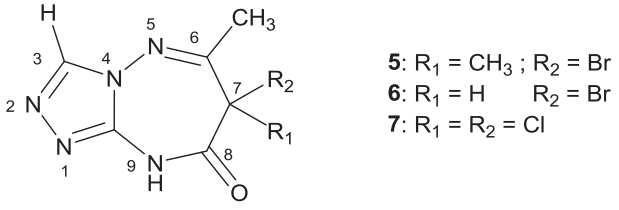

Scheme 3. Halogenated triazolotriazepines derivatives **5–7**.

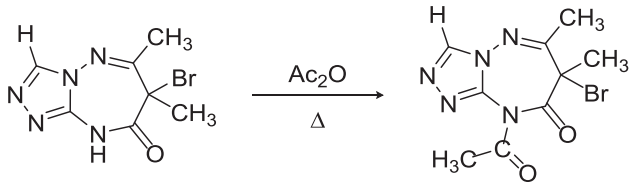

Scheme 4. Synthesis of monoacetylated compound **8**.

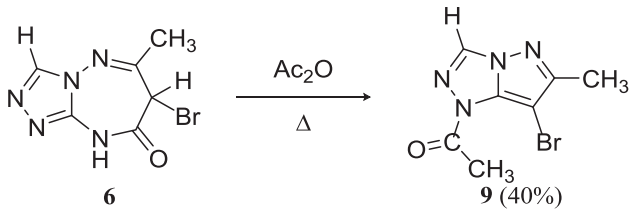

Scheme 5. Synthesis of compound **9** from **6**.

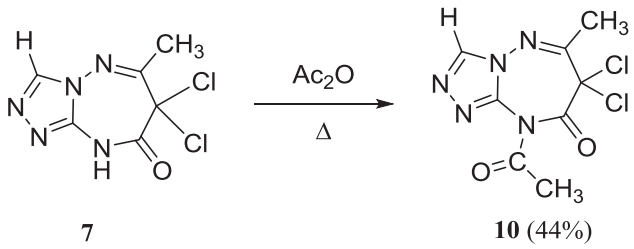

Scheme 6. Synthesis of compound **10.**

2.1. Thionation reaction

The thionation reaction of 6-methyl-7*H*[1,2,4]triazolo [4,3-b]triazepin-8(9*H*)-one was carried out by employing phosphorus pentasulfide under reflux in acetonitrile in the presence of sodium bicarbonate (Scheme 8).

In order to consider the influence of the presence of a thiolactam group in the seven-membered ring on the course of rearrangement previously described, it seems interesting to study the reaction involving acetic anhydride and 1,2,4-triazolo [4,3-b][1,2,4]triazepine-2-thione **11**. Thus, heating compound **11** in acetic anhydride made it possible to prepare compounds **12–15**, separable by silica gel column chromatography, namely azetopyrazolotriazole **12**, carbamylpyrazolotriazole **13**, cyanopyrazolotriazole **14** and pyrazolotriazole **15** (Scheme 9).

The structures of the compounds obtained were elucidated on the basis of spectral data (^{1}H NMR, ^{13}C NMR). Thus, in the ^{1}H NMR spectrum of **12**, we note in particular two signals at 2.40 and 2.14 ppm attributable to methyl groups at the position 3 of the tricyclic system and to the methyl group of acetyl, respectively. The signal at 9.03 ppm corresponds to the triazole proton in position 6. The ^{13}C NMR spectrum shows, in particular, the presence of a quaternary carbon at 105.56 ppm attributed to the carbon at position 9. The presence of the thiocarbonyl group is evidenced by the signal at 190.02 ppm. The ^{1}H NMR spectrum of **13** shows two signals at 2.59 and 2.40 ppm corresponding to the pyrazole and acetyl methyl groups, respectively. The two signals at 13.92 and 21.23 ppm correspond to methyl groups and a signal at 167.77 ppm correspond to the carbon of the thiocarbonyl group. The ^{1}H NMR spectrum of compound **14** shows, in particular, a signal at 2.34 ppm due to the methyl group attached to the pyrazole carbon and a signal at 9.06 ppm corresponding to the triazole proton. The ^{13}C NMR spectrum shows, in particular, a signal at 14.11 ppm attributable to the methyl group. Thus, the initial stage of the rearrangement reaction corresponds to acetylation of the N_1 nitrogen of the bicyclic system leading to the intermediate [D].

The abstraction of the hydrogen atom attached to the carbon in position 7 creates a carbanion which, according to a transannular reaction, attacks the carbon C_{9a} of the resulting iminium cation to give a tricyclic compound [E] which can evolve in two ways (Scheme 10). In the first, it stabilizes while evolving towards the conjugated tautomeric form **12**. According to a second route, the intermediate [E] undergoes an opening reaction of the β-thiolactam ring to yield the bicyclic compound **13**. The latter, under the conditions of the reaction, undergoes an intramolecular cyclization involving the sulfanyl group of the sulfanylimino group of the tautomeric form F, and the carbonyl of the acetyl group. The intermediate [G], thus formed, undergoes an opening reaction of the 1,3-thiazine nucleus to give the intermediate [H] which can stabilize in two ways (i) elimination of a molecule of thioacetic acid to give cyanopyrazolotriazole **14**, and (ii) loss of a molecule of acetyl thiocyanate to give the compound **15**.

2.2. Biological result

2.2.1. Antidiabetic activity assay

In the lumen of the small intestine, complex starch structures are broken down into oligosaccharides under α-amylase activity, whereas the membrane-bound intestinal α-glucosidases hydrolyze the resulting oligosaccharides, trisaccharides, and disaccharides into glucose and other monosaccharides. The inhibition of these enzymes reduces the rate of digestion of carbohydrates and consequently reduces the proportion of glucose in the blood [21]. In this context, to demonstrate the antidiabetic activity of the new compounds, we investigated their α-glucosidase and α-amylase inhibitory activities and the obtained results are compared in regards to the reference drug acarbose (Table 1). It is clearly noticed that all the novel molecules are potent α-glucosidase inhibitors compared to the standard acarbose. Out of the synthesized compounds, the triazepine derivative displayed the most potent activity with the lowest IC_{50} value of 141.13 ± 16.2 µM, compared to 309.11 ± 22.32 µM for the reference drug. Most of the compounds exhibited better IC_{50} values than acarbose, except compounds **2** and **11**. Furthermore, compounds **1**, **11** and **12** displayed high α-amylase inhibitory activities with IC_{50} of 126.52 ± 16.66 µM, 121.15 ± 35.65 µM and 109.43 ± 36.12 µM, compared to acarbose 618.87 ± 31.76 µM (5 folds better).

2.2.2. Molecular docking results

Molecular docking studies reveal that the inhibitory potency of the new compounds depends on the inhibited enzyme. Thus, the new compounds showed relatively potent inhibition against α-glucosidase with negative bonding energies, while no significant inhibition efficiency is obtained against α-amylase with zero bonding energy. Hence, our discussion of docked pyrazolotriazole derivatives results will be on the results obtained for the inhibition of α-glucosidase. The inhibition concentration values (IC_{50}) of pyrazolotriazole derivatives along with the acarbose drug as inhibitors of α-glucosidase are presented in Table 2. It is evident from the observed results that the inhibition efficiency depends on the geometrical structure and the position and nature of the substituent functional group in the new compounds. According to the inhibitory IC_{50} values of α-glucosidase inhibition (Table 2), **1** is the most active with lowest IC_{50} values of 141 µM and **2** is the least active compound with the highest IC_{50} values of 595 µM. Compounds **1** and **11** differ only by the functional group on C8, the former bears a ketone group (CO) and the latter bears a thione group (CS). This substitution of **1** by thione group (compound **11**) induces a significant decrease in the inhibition efficiency of **14** against α-glucosidase by half (Table 2). The derivatives **2** and **12–15** differ only by the substituent on the basic skeleton 1*H*-pyrazolo[5,1–c][1,2,4]triazole. For instance, **14** and **15** differ only by the substitution of the cyano group at C7 in the former. This substitution leads to an increase in the inhibition efficiency of **14** compared to **15** (Table 2). For a deeper

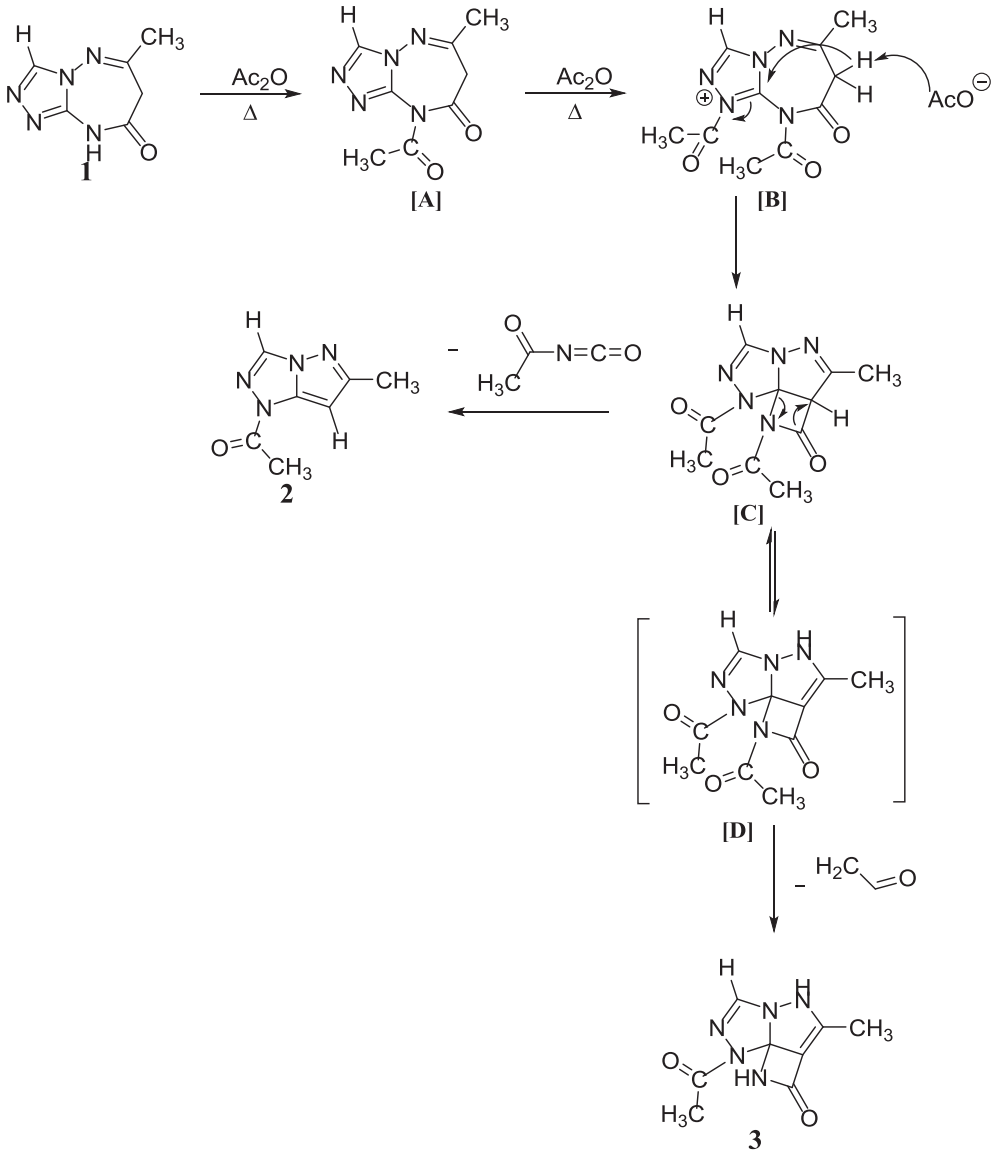

Scheme 7. Proposed mechanism for the synthesis of **2** and **3**.

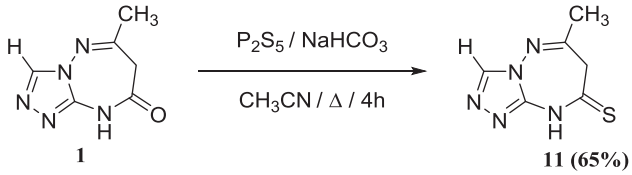

Scheme 8. Thionation reaction of 6-methyl-7*H*[1,2,4]triazolo [4,3-b]triazepin-8(9*H*)-one (1).

understanding of the experimental results and to rationalize the highest activity of **1** compared to **2**, **1** compared to **11**, and the low activity of **15** with regards to **14**, a molecular docking study has been carried out to shed light on the established binding modes of the chosen derivatives into the active site of *α*-glucosidase enzyme. Further, the inhibition efficiency of these compounds will be compared with the one of acarbose. Table 2 summarizes the calculated binding energies of the stable complexes ligand-β-*α*-glucosidase and the number of established intermolecular hydrogen bonding interactions between the compounds, the reference drug acarbose and the active site residues of *α*-glucosidase.

Fig. 1 shows different interaction modes involving the compound docked into the active site of *α*-glucosidase. From the docking results in Table 2 and Fig. 1, the highest activity of **1** compared to the least active one **2** is due mainly to (ii) the stability of the complex formed between the docked compound and *α*-glucosidase, (ii) the number of hydrogen bonding interactions (HB) established between the docked derivative and the active site residues of the *α*-glucosidase, and (iii) to the number of residues interacting with the docked ligand. Indeed, **1** has lowest binding energy (−8.24 kcal/mol) compared to **2** (−4.79) and a high number of HBs (three HBs) compared to **2** (two HBs) and finally, a high number of residues (eight amino acid) compared to **2** (four amino acids). In the stable complex formed between **1** and α-glucosidase, the strongest hydrogen bond is formed between the ASP202 amino acid and the hydrogen atom of the NH group of **1** with a distance of 2.15 Å. The second hydrogen bond is weaker than the first one and is established between the keto group of **1** and ARG200 with a distance of 2.96 Å. The third hydrogen bond is even weaker than the previous ones and it is established between the GLN110 amino acid and the nitrogen atom at position 2 of the triazol ring in **1** with a distance of 3.07 Å (Fig. 1). However, for derivative **2** the two hydrogen bonds are formed between the amino acid ARG400 and the N atom of the triazol ring and the keto group and are of distances 3.07 and 3.07 Å, respectively (Fig. 1). As mentioned above the derivatives **1** and **11** differ only by a keto or a

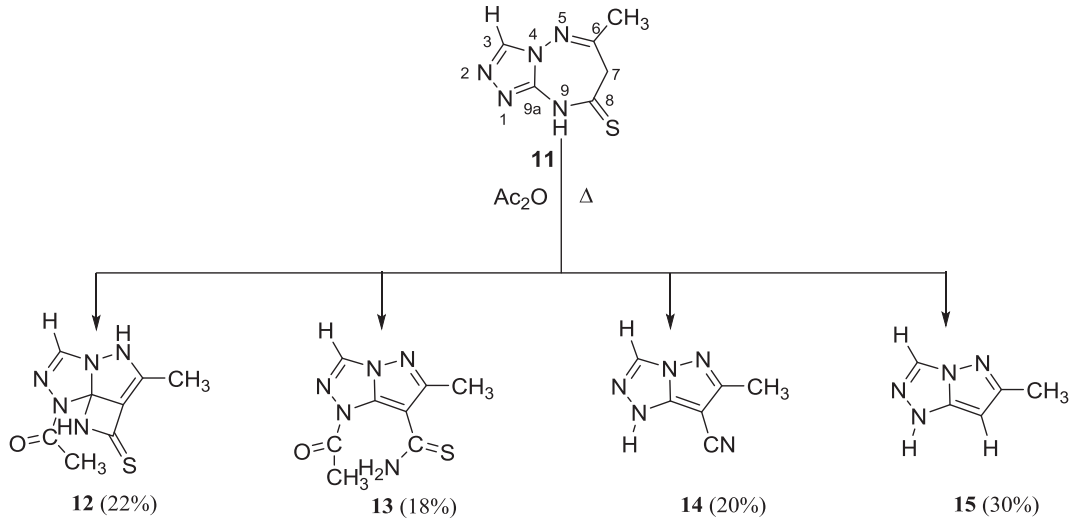

Scheme 9. The action of acetic anhydride on the compound **11**.

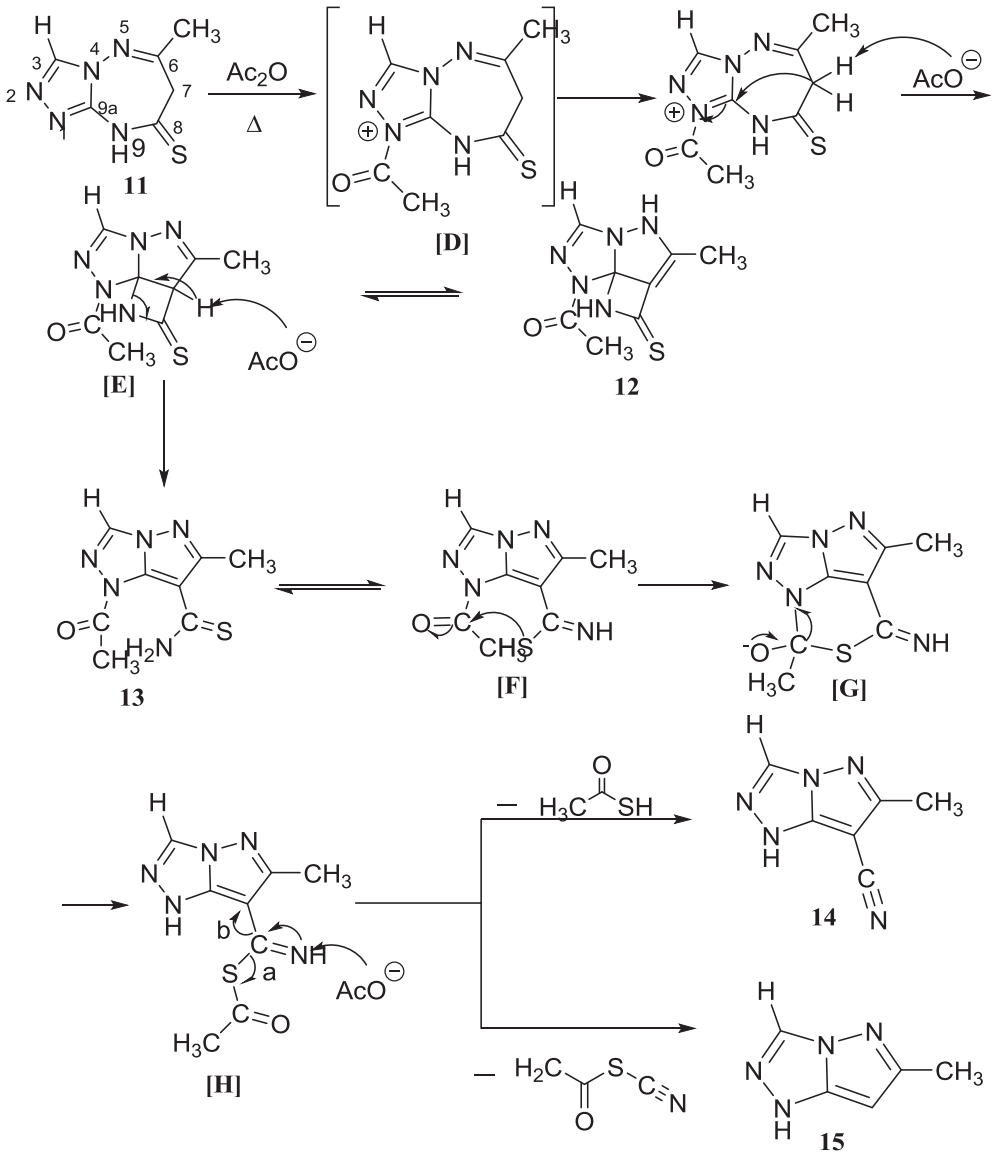

Scheme 10. Proposed mechanism of the formation of compounds **12–15.**

Table 1
Antidiabetic inhibitory of the synthesized compounds.

Compounds	Antidiabetic (IC_{50} in μM)	
	α-glucosidase	α-amylase
1	141.13 ± 16.2	126.52 ± 0.66
2	595.04 ± 43.42	260.40 ± 0.27
11	281.21 ± 30.23	425.17 ± 0.02
12	503.43 ± 35.11	121.15 ± 0.65
13	216.22 ± 17.32	764.56 ± 0.10
14	433.32 ± 88.31	219.89 ± 0.08
15	300.45 ± 47.87	109.43 ± 6.12
Acarbose	309.11 ± 22.32	618.87 ± 0.76

thione group at the C8 position, respectively. The substitution of the thione group for the keto group induces a decrease in enzyme inhibition by half (Table 2). The docking results show that both derivatives have similar interactions with the active sites that include close binding energies, the same number of HBs and residues that surround the docked ligand (Table 2). However, the main difference is found in the lengths of the hydrogen bonds formed between the keto and thione groups with the ARG200 amino acid. For **1**, this distance is 2.96 Å but for **9** it is 3.32 Å. One can conclude that the higher activity of **1** compared to **11** is mainly to the stronger hydrogen bond formed between ARG200 and the keto group compared that formed to the thione group. In a similar way, the higher activity of **15** compared to **14** may be explained by (i) the high number of hydrogen bonds formed between **15** and the residues of α-glucosidase in the active site and to the number of residues surrounding **12** in the active site (Table 1). For instance, in the complex formed between **15** and α-glucosidase three hydrogen bonds are established between docked **12** and the residues in the active site while in the complex formed between **14** and α-glucosidase two hydrogen bonds are established to residues in the active site (Table 2).

According to the observed *α*-glucosidase inhibition results in Table 2, the reference drug acarbose shows lower inhibition efficiency than **1** and **11**; and higher inhibition than **2** and **14** compounds. The docked reference drug acarbose into the active site is thermodynamically favorable with a binding energy of −10.56 kcal/mol. The stability of acarbose-α-glucosidase complex is mainly referred to the strong intermolecular hydrogen bonding formed between the hydroxyl group of acarbose and the active residue of α-glucosidase (Fig. 1). Indeed, ten intermolecular hydrogen bonds are formed between acarbose and the active residues of α-glucosidase (Fig. 1). The reference drug acarbose has a different basic skeleton than the sets of compounds (**1** and **11**) and (**2**, **14** and **15**). Therefore, molecular docking results in Table 2 may not help in comparing the observed result of the reference drug acarbose and those of the sets of compounds (**1** and **11**) and (**2**, **14** and **15**). In one hand, one can easily deduce that the higher activity of acarbose compared with **2** and **15** may refer to (i) the stability of acarbose-α-glucosidase complex compared with the ones formed with **2** and **15**; and (ii) number of hydrogen bonds formed with acarbose compared with the ones formed with **2** and **15**(Fig. 1). In another hand, docking results may not explain the higher activity of **1** and **11** compared with the one of the acarbose. The higher activity of **1** and **11** compared with the one of the acarbose may probably due to the basic skeleton structure itself.

2.2.3. Molecular dynamics results

After the biological screening and docking results, the best binding pose of 6-methyl7*H*[1,2,4]triazolo [4,3-b][1,2,4]triazepin-8(9*H*)-one (thione) (**11**) in complex with *α*-glucosidase was subjected for molecular dynamics simulation to understand the stability of **11** in the *α*-glucosidase microenvironment. Fig. 2a and b shows the Root Mean Square deviation (RMSD) and Root Mean Square Fluctuation (RMSF) of compound **11**- *α*-glucosidase complex.

The RMSD of protein backbone (Cα) and the ligand is useful to understand the structural conformation of compound **11** in the α-glucosidase complex. RMSD analysis can also indicate the simulation equilibration and its fluctuation for compound **11**- *α*-glucosidase complex throughout the end of the simulation. In general, 1–3 Å structural fluctuations represent the small, globular protein confirmation. In Fig. 2(a) RMSD results of compound **11**- *α*-glucosidase complex confirms that which is perfectly acceptable for small, globular protein confirmation [23]. Also, Fig. 2a (Lig fit Prot (**Ligand fitting on protein)**) shows that **11** binding was stable in the *α*-glucosidase system throughout the simulation. Fig. 2b RMSF is useful to characterizing local changes along the *α*-glucosidase protein chain. From that Fig. 2b, peaks indicate areas of the *α*-glucosidase protein that fluctuate the most during the simulation, secondary structure elements like alpha helices and beta strands are usually more rigid than the unstructured part of the protein, and thus fluctuate less than the loop regions. Protein active site residues that interact with the compound **11** are marked with green-colored vertical bars (Fig. 2b).

As mentioned in Fig. 3a Protein interactions with the ligand was monitored throughout the simulation from that figure ARG 200 residue is having a high probability of interaction with *α*-glucosidase, the values over 1.0 are possible as some protein residue may make multiple contacts of the same subtype with the compound **11**. Fig. 3b shows the detailed ligand atom interactions with the protein residues [24].It is possible to have interactions with > 100% as some residues may have multiple interactions of a single type with the same ligand atom. For example, the ARG side chain has four H-bond donors that can all hydrogen-bond to a single H-bond acceptor.

In addition to this, the interactions and contacts of (H-bonds, Hydrophobic, Ionic, Water bridges) of compound **11** – *α*-glucosidase complex monitored during the simulation as shown in Fig. 4. The top panel shows the total number of specific contacts the protein makes with the ligand over the course of the trajectory. The bottom panel shows which residues interact with the ligand in each trajectory frame. Some residues make more than one specific contact with the ligand, which is represented by a darker shade of orange, according to the scale to the right of the plot. The molecular dynamics result concludes that compound **11** is very stable in the *α*-glucosidase system and which supports the above experimental results.

Table 2
Docking binding energies, number of hydrogen bonding interactions and number of closest residues to the docked compounds and acarbose within the active binding site of *α*-glucosidase.

Name of synthesized derivatives	Free binding energy (kcal/mol)	H-Bonds (HBs)	Number of closest residues to the docked ligand in the active site	IC_{50} ± SEM
α-glucosidase				
1	−8.24	3	8	141.13 ± 16.2
2	−4.79	2	4	595.04 ± 43.42
11	−8.04	3	7	281.21 ± 30.23
14	−5.44	2	5	433.32 ± 88.31
15	−4.81	3	9	300.45 ± 47.87
Acarbose	−10.56	10	10	309.11 ± 22.32

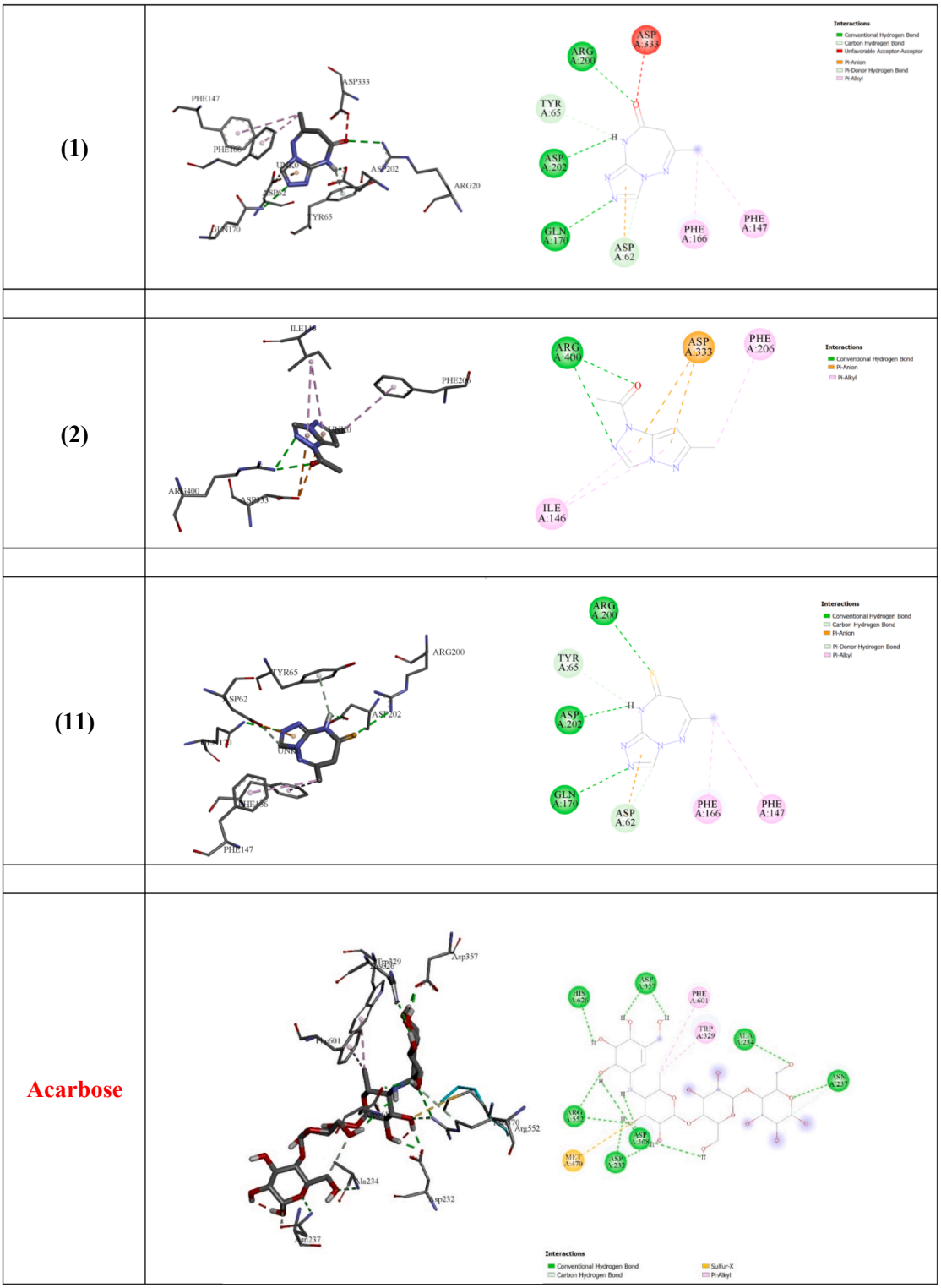

Fig. 1. 3D (right) and 2D (left) closest interactions between active site residues of α-glucosidase and compounds **1**, **2**, **11** and acarbose.

2.2.4. Antioxidant activities of the synthesized compound

The *in vitro* antioxidant activity of the new compounds is evaluated by DPPH and ABTS radical scavenging methods and the ferric reducing antioxidant power assay. The results are summarized in Table 3 and expressed in trolox or ascorbic acid equivalents. Among the compounds screened, compound **11** having a sulfur atom in the triazepine ring showed the highest radical scavenging (DPPH: 0.546 ± 0.006 µmol TE/mol and ABTS: 3.245 ± 0.081 mmol TE/mol) and ferric reducing ability (32.688 ± 0.109 µmol AAE/mol), which might be due to the presence of sulphur group. On the other hand, the compound **14** exhibited the lowest antioxidant effect.

2.2.5. DFT results

The antioxidant activity of the new compounds to scavenge the

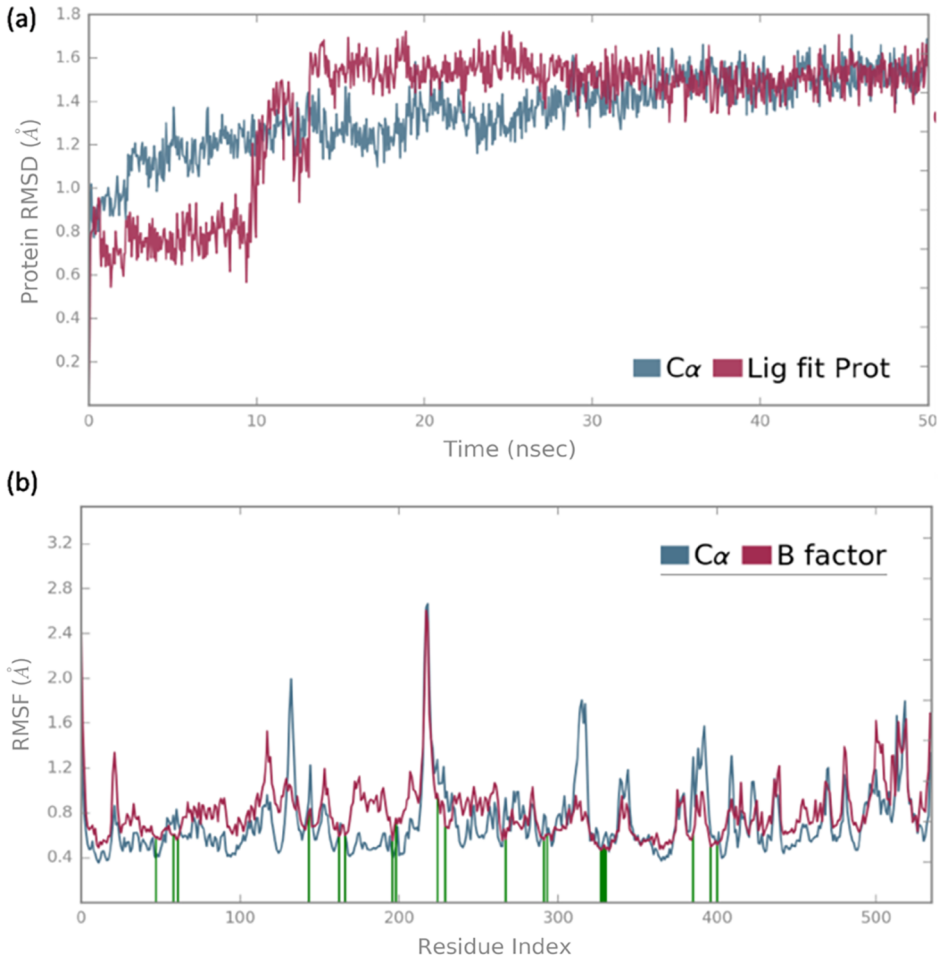

Fig. 2. (a) RMSD (b) RMSF of compound **11**- *α*-glucosidase complex during 50 ns.

DPPH (2,2-Diphenyl-1-picrylhydrazyl) free radical was determined as described in the methodology section. On the basis of the data in Table 3, the new compounds show the ability to scavenge DPPH free radical. To rationalize and explain the observed antioxidant activity of the new compounds, the bond dissociation enthalpies (BDE) of the X—H bonds (X=C or N) of An—H (An—H is for antioxidant compound) and ionization potentials of An—H were calculated at the B3P86/6-311 + + G(d,p) level of theory (Table 4). The solvent effects are taken into account implicitly using the polarizable continuum model. By comparing the BDE values in Table 4 for all of the new compounds, it is evident that the homolytic bond dissociation is more favorable for N—H (BDE values lower than 100 kcal/mol) than C—H bonds (BDE values higher than 120 kcal/mol). However, **2** and **11** have no NH group in their chemical structures. This allows us to conclude that the radical scavenging ability of these two compounds is governed by another parameter which we suggest is ionization potential (IP). Indeed, by comparing IP values of **15** and **2** it is obvious that the high activity of **13** compared to **2** is mainly due to the lower IP value of **13** (6.87 eV) compared to **2** (7.27 eV). Compounds **1** and **11** differ only by the type of functional group at C8 (Schemes 2 and 8). By considering only those with an NH group, one can divide the results according to the basic skeleton. Thus, **1** and **13** form the first class, the second class contains **14** and **15** and the final class only **12**. For the first class, it is found experimentally that **11** (the most active compound) shows higher activity than **1**. This result is in accordance with lower BDE and IP values for the former compared to the latter. Similarly, the lower BDE and IP values explain the high activity of **15** compared to **11**. The effect of aprotic solvent was investigated by calculating the BDEs of 3-CH group of **1** in dimethylsulfoxide using PCM model. The effect is found negligible with a BDEs variation less than 0.01 compared with those obtained in methanol. This weak influence is in accordance with the previous results reported by Kosinova et al. [25].

3. Conclusion

In summary, we have synthesized via original rearrangements several condensed 1,2,4-triazole compounds with biologically interesting activities, involving 6-methyl7*H*[1,2,4]triazolo [4,3-b][1,2,4]triazepin-8(9*H*)-one(thione) and acetic anhydride. The structure of the new heterocyclic ring systems was proved by spectroscopic methods and single-crystal X-ray diffraction. Plausible mechanisms of these reactions have been proposed and discussed. We have shown that the presence of a hydrogen atom in position 9 of the bicyclic compounds is necessary for observing the ring transformation of the seven-membered rings. It was possible for us to highlight for the first time a new condensed triazole compound containing a β-lactam moiety. The new compounds showed high antidiabetic activities compared to the antidiabetic agent acarbose and furthermore exhibited moderate to low antioxidant activities. Molecular docking and molecular dynamics study showed the extent of inhibition by the new compounds against α-glucosidase is mainly due to the number and the strength of H-bonds, Ionic, Water bridges between the docked compound and active residues of the enzyme in the active site. BDEs and IPs calculated at DFT level of theory showed that the radical scavenging capacity of the new compounds depends on their basic skeleton and the type of the substituent functional groups on it. Those results suggest the interesting medical properties of those molecules, which will be subject of *in vivo* toxicological and pharmacological studies.

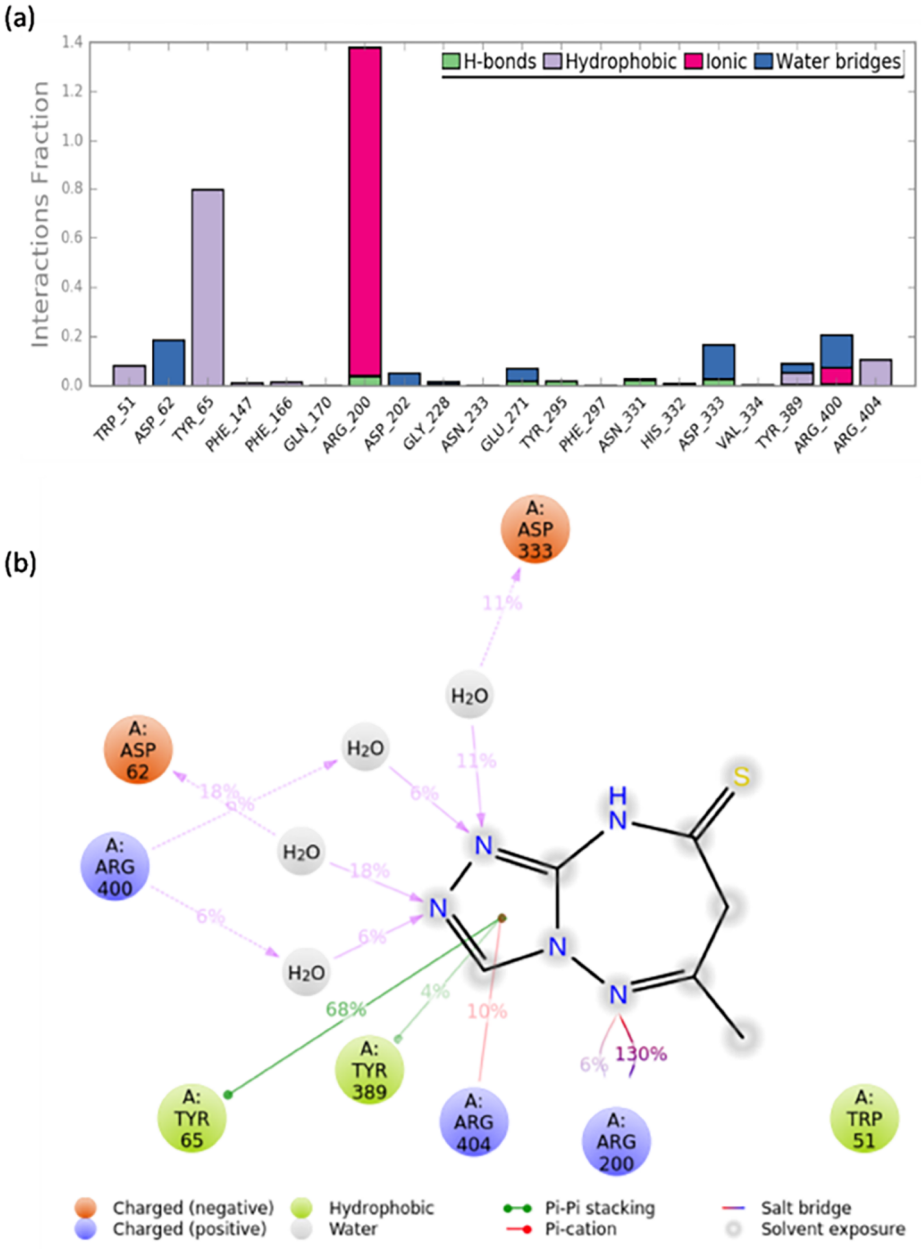

Fig. 3. (a) Protein-ligand interaction fraction (b) detailedligand atom interactions with the protein residues.

4. Material and methods

4.1. Chemistry synthesis

The NMR spectra were measured on a BrukerAvance DPX300 instrument. The chemical shifts (δ) are expressed in ppm down field from TMS taken as an internal reference. Mass spectra were performed on a Perkin-Elmer SCIEX API unit 300. The samples are ionized by the ion spray technique (IS). TLC and column chromatography were carried out respectively on silica plates (Merck 60 F254) and silica gel (Merck 60, 230–400 mesh).

Synthesis of 6-methyl-7H,8H,9H-[1,2,4]triazolo [4,3-b][1,2,4]*triazepin-8-one* ***(1)***

In a flask containing 10 mL of ethyl acetylacetate (0.02 mol), 2 g of sodium acetate (0.024 mol) 3.6 g (0.02 mol) of 3,4-diamino[1,2,4]triazolehydrobromide was heated under reflux during 3 h. After cooling, the precipitate formed was filtered off under vacuum and the mixture was washed with ethanol.

White solid, yield: 70%; m.p: 256–258 °C, ^{1}H NMR (DMSO-d_6, 300 MHz) δ 2.28 (s, 3H, CH_3); 3.55 (s, 2H, CH_2); 8.71 (s, 1H, $CH_{triazolic}$).^{13}C NMR (DMSO-d_6, 75 MHz) δ 24.94 (CH_3); 42.8437 (−CH_2−); 141.42 (−CH−); 144.08 (C═N); 164.78 (C═N); 168.99 (C═O). HRMS (ESI) Calculated for C6H7N5O: [M + H$^+$] = 165.0717, Found: [M + H$^+$] = 165.0716. Elemental analysis Calculated: C, 43.63%; H, 4.27%; N, 42.41%; O, 9.69%, Found: C, 43.62%; H, 4.26%; N, 42.40%; O, 9.70%.

Synthesis of 1-acetyl-6-methyl-pyrazolo[3,2–c][1,2,4]triazole ***(2)***

1g of **1** was heated in 8 mL of acetic anhydride for 15 min. The solution was then concentrated to dryness under reduced pressure and the residue was extracted with dichloromethane under pressure. The precipitate was chromatographed on a silica column (eluent: dichloromethane/methanol 95/5 v / v). By which two products (**2** and **3**) were obtained.

Colourless crystals yield: 60%; m.p: 143–145 °C. ^{1}H NMR (300 MHz, $DMSOd_6$) δ ppm: 8.52(s, 1H, N═CH); 6.15 (s, 1H, C═CH); 2.69(s, 3H, CH_3); 2.25 (s, 3H, CH_3).^{13}C NMR (75 MHz, $DMSOd_6$) δ ppm: 162.74,

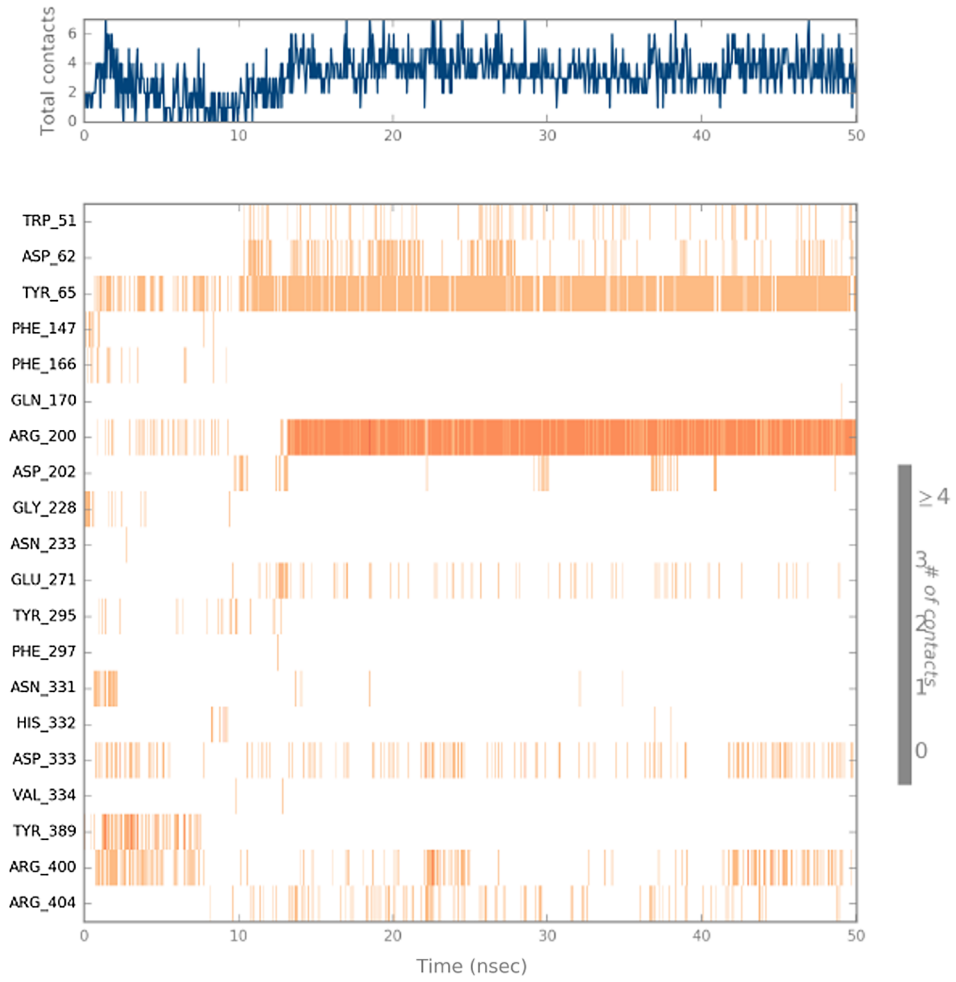

Fig. 4. shows the timeline representation of the interactions and contacts (H-bonds, Hydrophobic, Ionic, Water bridges) of compound 11 - *α*-glucosidase complex.

Table 3
Antioxidant activity of the new compounds.

Compounds	Antioxidant assays		
	DPPH µmol TE/mol	ABTS mmol TE/mol	FRAP µmol AAE/mol
1	0.241 ± 0.002	0.705 ± 0.014	1.650 ± 0.007
2	0.066 ± 0.010	0.058 ± 0.003	0.038 ± 0.003
11	0.546 ± 0.006	3.245 ± 0.081	32.688 ± 0.109
12	0.0521 ± 0.006	0.050 ± 0.004	0.181 ± 0.005
13	0.119 ± 0.007	0.209 ± 0.001	1.829 ± 0.0065
14	0.023 ± 0.009	0.012 ± 0.002	0.180 ± 0.004
15	0.115 ± 0.004	0.076 ± 0.003	1.196 ± 0.001

150.78, 148.20Cq; 144.50, 100.33 (CH); 23.85, 13.87 (CH_3). HRMS (ESI) Calculated for $C_7H_8N_4O$: $[M+H^+] = 165.0699$, Found: $[M+H^+] = 165.0698$. Elemental analysis Calculated: C, 51.21%; H, 4.91%; N, 34.13%; O, 9.75%, Found: C, 51.19%; H, 4.90%; N, 34.14%; O, 9.73%.

Synthesis of 1-acetyl-6-methyl-7-oxo-1(5)-yl-7,8-dihydroazeto [3′,2′:4,5]pyrazolo[5,1–c][1,2,4]triazole ***(3)***

White solid, yield: 32%; m.p: 177–179 °C.^{1}H NMR (300 MHz, DMSO) δ ppm: 13.68(s, 1H, NH); 9.96(s, 1H, NH); 8.97(s, 1H, CH); 2.43(s, 3H, CH_3); 2.22(s, 3H, CH_3).^{13}C NMR (75 MHz, DMSO) δppm: 13C NMR (75 MHz, DMSO) δppm: 171.76, 161.79, 159.87, 146.36, 90.70 (Cq); 129.91 (CH); 25.38, 15.46(CH_3). HRMS (ESI) Calculated for $C_8H_9N_5O_2$: $[M+H^+] = 208.0829$, Found: $[M+H^+] = 208.0898$. Elemental analysis Calculated: C, 46.38%; H, 4.38%; N, 33.80%; O, 15.44%, Found: C, 46.39%; H, 4.40%; N, 33.79%; O, 15.43%.

Table 4
BDEs of pyrazolotriazole derivatives calculated at the PCM-B3P86/6"-311 + + G(d,p) level of theory.

Compound	IP	1-NH	3-CH	5-NH	7-CH	9-NH	Radical scavenging (µmol TE/mol)
1	−7.81	–	121.25	–	–	98.27	0.241 ± 0.002
2	−7.27	–	122.78	–	123.01	–	0.066 ± 0.010
11	−7.29	–	121.53	–	–	93.28	0.546 ± 0.006
12	−6.79	–	113.86	73.12	–	–	0.0521 ± 0.006
13	−6.87	–	123.10	–	–	–	0.119 ± 0.007
14	−7.28	94.17	124.66	–	–	–	0.023 ± 0.009
15	−6.75	87.72	123.37	–	123.58	–	0.115 ± 0.004

Synthesis of 7-bromo-6,7-dimethyl-7H-[1,2,4]triazolo [4,3-b][1,2,4] *triazepin-8(9H)-one* ***(5)***

White solid, yield: 25%; m.p: 294–296 °C. ^{1}H NMR (300 MHz, DMSO) δ ppm: 13.08(s, 1H, NH); 8.97(s, 1H, CH); 2.43(s, 3H, CH_3); 2.21(s, 3H, CH_3).^{13}C NMR (75 MHz, DMSO) δppm: 172.74, 160.83, 146.32, 80.70 (Cq) ; 139.91 (CH); 22.35, 15.30(CH_3). HRMS (ESI) Calculated for $C_7H_8N_5OBr$: $[M+H^+]$ = 256.9879, Found: $[M+H^+]$ = 256.9880. Elemental analysis Calculated: C, 32.58%; H, 3.12%; N, 27.14%; O, 6.20%; Br, 30.96%, Found: C, 32.60%; H, 3.14%; N, 27.11%; O, 6.19%; Br, 30.95%.

Synthesis of 7-bromo-6-methyl-7H-[1,2,4]triazolo [4,3-b][1,2,4]*triazepin-8(9H)-one* ***(6)***

White solid, yield: 22% m.p: 180–182 °C. ^{1}H NMR (300 MHz, DMSO) δ ppm: 13.10 (s, 1H, NH); 8.96(s, 1H, =CH);4.56(s, 1H, CH); 2.22(s, 3H, CH_3).^{13}C NMR (75 MHz, DMSO) δppm : 169.56, 160.89, 146.36, (Cq); 78.63, 138.15 (CH); 15.43(CH_3).HRMS (ESI) Calculated for $C_6H_6N_5OBr$: $[M+H^+]$ = 242.9899, Found: $[M+H^+]$ = 256.9898. Elemental analysis Calculated: C, 29.53%; H, 2.48%; N, 28.70%; O, 6.56%; Br, 32.74%, Found: C, 29.52%; H, 2.47%; N, 28.69%; O, 6.55%; Br, 32.75%.

Synthesis of 7,7-dichloro-6-methyl-7H-[1,2,4]triazolo [4,3-b][1,2,4] *triazepin-8(9H)-one* ***(7)***

White solid, yield: 25%; m.p: 182–184 °C. ^{1}H NMR (300 MHz, DMSO) δ ppm: 13.12(s, 1H, NH); 8.94(s, 1H, CH); 2.20 (s, 3H, CH_3).^{13}C NMR (75 MHz, DMSO) δppm: 166.76, 161.79, 146.16, 110.70 (Cq) ; 139.11 (CH); 12.16(CH_3).HRMS (ESI) Calculated for $C_6H_5N_5OCl_2$: $[M+H^+]$ = 232.9997, Found: $[M+H^+]$ = 232.9996. Elemental analysis Calculated: C, 30.79%; H, 2.15%; N, 29.92%; O, 6.84%; Cl, 30.30%, Found: C, 30.80%; H, 2.14%; N, 29.91%; O, 6.83%; Cl, 30.29%.

Synthesis of 6,7-dimethyl-9-acetyl-7-bromo-8,9-dihydro[1,2,4]triazolo [4,3-b][1,2,4]*triazepin-8-one* ***(8)***

White solid, yield: 36%; m.p: 160–161 °C. ^{1}H NMR (300 MHz, $DMSOd_6$) δ ppm: 8.53 (s, 1H, N = CH); 2.32 (s, 3H, CH_3); 2.26 (s, 3H, CH_3); 2.06 (s, 3H, CH_3).^{13}C NMR (75 MHz, $DMSOd_6$) δ ppm179.30, 173.11, 160.68, 157.02, 51.94 (Cq); 138.72 (CH); 26.37, 24.09, 19.31(CH_3). HRMS (ESI) Calculated for $C_9H_{10}N_5O_2Br$: $[M+H^+]$ = 300.0089, Found: $[M+H^+]$ = 300.0091. Elemental analysis Calculated: C, 36.02%; H, 3.36%; N, 23.34%; O, 10.66%; Br, 26.62 Found: C, 36.01%; H, 3.35%; N, 23.32%; O, 10.65%, Br, 26.60%.

Synthesis of 1-acetyl-7-bromo-pyrazolo[3,2–c][1,2,4]triazole ***(9)***

0.5 g of 4 was heated in 8 mL of acetic anhydride for 1 h. After cooling, the precipitated product is filtered.

White solid, yield: 40%; m.p: 178–180 °C. ^{1}H NMR (300 MHz, $DMSOd_6$) δ ppm: 8.52(s, 1H, N = CH); 2.74 (s, 3H, CH_3); 2.34(s, 3H, CH_3).^{13}C NMR (75 MHz, $DMSOd_6$) δ ppm: 163.86, 146.00, 143.31, 141.82 (Cq); 89.84(CH); 23.85(CH_3); 14.03(CH_3). HRMS (ESI) Calculated for $C_9H_{10}N_5O_2Br$: $[M+H^+]$ = 300.0089, Found: $[M+H^+]$ = 300.0091. Elemental analysis Calculated: C, 36.02%; H, 3.36%; N, 23.34%; O, 10.66%; Br, 26.62 Found: C, 36.01%; H, 3.35%; N, 23.32%; O, 10.65%, Br, 26.60%.

Synthesis of 6-methyl-9-acetyl-7,7-dichloro-8,9-dihydro[1,2,4]triazolo [4,3-b][1,2,4]*triazepin-8-one* ***(10)***

0.5 g of compound **5** was heated in 10 mL of acetic anhydride for 1 h, the solution concentrated with an air stream and the residue taken up in ether followed by filtration of the precipitated product.

White solid, yield: 44%; m.p: 190–192 °C. ^{1}H NMR (300 MHz, $DMSOd_6$) δ ppm: 8.71(s, 1H, N = CH); 2.45 (s, 3H, CH_3); 2.32(s, 3H, CH_3).^{13}C NMR (75 MHz, $DMSOd_6$) δ ppm: 173.34, 163.30, 158.59, 156.06, 75.57 (Cq); 139.91 (CH); 24.94(CH_3); 23.39(CH_3). HRMS (ESI) Calculated for $C_8H_7N_5O_2Cl_2$: $[M+H^+]$ = 276.0899, Found: $[M+H^+]$ = 276.0897. Elemental analysis Calculated: C, 34.80%; H, 2.56%; N, 25.37%; O, 11.59%; Cl, 25.68 Found: C, 34.79%; H, 2.53%; N, 25.32%; O, 11.61%, Cl, 25.67%.

Synthesis of 6-methyl-7H-[1,2,4]triazolo [4,3-b][1,2,4]*triazepin-8(9H)-thione* ***(11)***

A solution of **1** (2 g) and phosphorus pentasulfide (2.2 g) in 40 mL of acetonitrile to which a pinch of sodium bicarbonate was added was heated at gentle reflux for 4 h and then evaporated to dryness. The residue was taken up in 20 cm^3 of boiling water and the precipitate which formed on cooling was filtered off.

Yellow solid, yield: 65%; m.p: 219–221 °C. ^{1}H NMR (DMSO-d_6, 300 MHz) δ 2.27(s, 3H, CH_3), 3.98(2H, $-CH_2-$), 8.83(s, 1H, $C-H_{triazolic}$); ^{13}C NMR (DMSO-d_6, 75 MHz) δ 24.34, 51.90, 141.70, 190.31. HRMS (ESI) Calculated for $C_6H_7N_5S$: $[M+H^+]$ = 182.0409, Found: $[M+H^+]$ = 182.0410. Elemental analysis Calculated: C, 39.78%; H, 3.89%; N, 38.65%; S, 17.69%. Found: C, 39.77%; H, 3.90%; N, 38.63%; S, 17.67%.

The action of acetic anhydride on compound ***(13)***

1 g of **10** was heated in 10 mL of acetic anhydride for 1 h. The solution was then concentrated to dryness under reduced pressure and the residue was extracted with dichloromethane under pressure. The precipitate was chromatographed on a silica column (eluent: dichloromethane/methanol 95/5 v / v). By which four products (**12**, **13**, **14** and **15**) were obtained.

1-acetyl-6-methyl-7-thiooxo-1(5)-yl-7,8-dihydroazeto[3′,2′:4,5]pyrazolo[5,1–c][1,2,4]triazole ***(12)***

Off-white solid, yield: 22%; m.p: 214–216 °C .^{1}H NMR (300 MHz, DMSO) δppm: 13.92 (s, 1H, NH); 10.95(s, 1H, NH); 9.03(s, 1H, CH); 2.40(s, 3H, CH_3); 2.14(s, 3H, CH_3).^{13}C NMR (75 MHz, DMSO) δ ppm: 190.32, 168.66, 158.42, 147.46, 105.60 (Cq); 130.39 (CH); 24.69, 16.29 (CH_3). HRMS (ESI) Calculated for $C_8H_9N_5OS$: $[M+H^+]$ = 224.0519, Found: $[M+H^+]$ = 224.0520. Elemental analysis Calculated: C, 43.04%; H, 4.06%; N, 31.37%; O, 7.17%; S, 14.36%. Found: C, 43.02%; H, 4.05%; N, 31.38%; O, 7.15%; S, 14.37%.

7-carbothioamide-1-acetyl-6-methyl-1H-pyrazolo[5,1–c][1,2,4]triazole ***(13)***

Off-white solid, yield: 18%; m.p: 202–204 °C ^{1}H NMR (300 MHz, DMSO) δ ppm: 9.34(s, 1H, CH); 2.59 (s, 3H, CH_3); 2.40 (s, 3H, CH_3).^{13}C NMR (75 MHz, DMSO) δ ppm: 167.77, 161.78, 143.57, 113.44, 73.40 (Cq); 133.23 (CH); 21.23, 13.92(CH_3).

Synthesis of 7-carbonitrile-6-methyl-1H-pyrazolo[5,1–c][1,2,4]triazole ***(14)***

White solid, yield: 20%; m.p: 188–190 °C. ^{1}H NMR (300 MHz, DMSO) δ 9.06 (s, 1H, CH); 2.34(s, 3H, CH_3).^{13}C NMR (75 MHz, DMSO) δ ppm: 160.91, 147.43, 114.84, 64.48 (Cq); 130.78 (CH); 13.98(CH_3). HRMS (ESI) Calculated for $C_6H_5N_5$: $[M+H^+]$ = 148.0616, Found: $[M+H^+]$ = 148.0617. Elemental analysis Calculated: C, 48.98%; H, 3.43%; N, 47.60%. Found: C, 48.97%; H, 3.44%; N, 47.59%.

Synthesis of 6-methyl-1H-pyrazolo[5,1–c][1,2,4]triazole ***(15)***

White solid, yield: 30%; m.p: 182–184 °C. ^{1}H NMR (300 MHz, DMSO) δppm: 12.57 (s, 1H, NH); 8.70(s, 1H, N=CH); 5.52(s, 1H, C=CH); 2.22(s, 3H, CH_3).^{13}C NMR (75 MHz, DMSO) δppm: 157.23, 147.39 (Cq); 128.91, 76.69 (CH); 15.16(CH_3). HRMS (ESI) Calculated for $C_5H_6N_4$: $[M+H^+]$ = 123.0621, Found: $[M+H^+]$ = 123.0619. Elemental analysis Calculated: C, 49.18%; H, 4.95%; N, 45.88%. Found: C, 49.18%; H, 4.94%; N, 45.89%.

4.2. Antidiabetic inhibition assays

The α-amylase inhibition assay was conducted according to the previously described protocol. Briefly, 20 μL of the sample was mixed with 230 μL of PBS and 250 μL of α-amylase (240 U/mL, in 0.02 M phosphate buffer, pH 6.9, with 0.006 M NaCl). After incubating at 37 °C for 10 min, 250 μL of 1% (w/v) soluble starch (in 0.02 M phosphate buffer, pH 6.9) was added and the mixture was further incubated at 37 °C for 30 min followed by adding 250 μL of DNS color reagent. Afterward, the reaction was stopped by heating in a boiling water bath for 10 min then cooling to room temperature. The mixture has been diluted with 2 mL of buffer and the absorbance was measured at 540 nm. As described previously, the α-glucosidase enzyme (0.1 U/mL) and substrate *p*-nitrophenyl-α-D-glucopyranoside (*p*-NPG, 1 mM) were

dissolved in potassium phosphate buffer (0.1 M, pH 6.7) and all samples were dissolved in Dimethyl sulfoxide. The inhibitor (20 µL) was pre-incubated with the enzyme (100 µL) and PBS (130 µL) at 37 °C for 10 min and then the substrate (200 µL) was added to the reaction mixture. The enzymatic reaction was performed at 37 °C for 30 min. The reaction was then terminated by the addition of 1.0 mL of 1.0 M Na_2CO_3. All samples were analyzed in triplicate with different concentrations to determine the IC_{50} values and the absorbance was recorded at 405 nm.

4.3. Antioxidant activities

The free radical scavenging activity of the compounds was measured by 2,2′-Diphenyl-1-picrylhydrazyl hydrate (DPPH). The ferric ions (Fe^{3+}) reducing antioxidant power (FRAP) method was used to measure the reducing capacity of the compounds. The reducing power of the extracts was represented as ascorbic acid equivalent (µmol of AAE/mol of the compound). The antioxidant activities samples are expressed as TEAC values, defined as the concentration of standard Trolox with the same antioxidant capacity of the extract under investigation (µmol of TE/g of the compound).

4.4. Computational details

4.4.1. Molecular docking study

The interaction binding modes between the active site residues of the enzymes (α-glucosidase and α-amylase) and the docked new pyrazolotriazole derivatives have been carried out using the Autodock package [26]. X-ray coordinates of α-glucosidase, α-amylase and their originated docked ligands were downloaded from the RCSB data bank website (PDB codes 3WY2 and 5EMY) [27,28]. As a first step, water molecules were removed and polar hydrogen atoms and Kollman charges were added to the extracted receptor structures of α-glucosidase and α-amylase by using the automated tool in AutoDock Tools 4.2. The active sites are identified based on co-crystallized receptor-ligand complex structures of α-glucosidase and α-amylase enzymes. The re-docking of the original ligands into the active site are well reproduced with an RMSD value of 0.66 and 1.72 Å for original ligands of α-glucosidase and α-amylase, respectively. 3D molecular structure geometries of pyrazolotriazole derivatives were minimized at a Merck molecular force field 94 (MMFF94) level44. The optimized geometries were saved as PDB files. Nonpolar hydrogens were merged and rotatable bonds were defined for each docked ligand. Docking studies were performed by using the Lamarckian genetic algorithm approach with 500 as a total number of runs for binding site for original ligands and 100 runs for each new pyrazolotriazole derivative. In each respective run, a population of 150 individuals with 27,000 generations and 250,000 energy evaluations were employed. Operator weights for crossover, mutation, and elitism were set to 0.8, 0.02, and 1, respectively. The binding site was defined using a grid of 40 × 40 × 40 points each with a grid spacing of 0.375 Å. The docking calculations have been carried out using an Intel (R) Core (TM) i5-3770 CPU @ 3.40 GHz workstation.

4.4.2. DFT calculations

It is reported that natural and synthetic antioxidant compounds (An−H) scavenge free radicals ($R^{\bullet}$) through hydrogen atoms transfer from the antioxidant to the free radical. Four main mechanisms have been proposed including (i) Proton Coupled-Electron Transfer (PC-ET) versus Hydrogen atom transfer (HAT), (ii) Electron Transfer-Proton Transfer (ET-PT), Sequential Proton Loss Electron Transfer (SPLET), and Adduct formation (AF) [29]. It is reported that the reactivity of the most antioxidants towards free radicals (e.g., $CH_3OO^{\bullet}$) involve a PC-ET mechanism [30,31]. Therefore, one can consider that the present compounds proceed through the same mechanism toward DPPH free radical (Eq. (1)):

$$An{-}H + R^{\bullet} \rightarrow An^{\bullet} + RH \quad (1)$$

In the above mechanism (Eq. (1)), the An−H bond dissociation is homolytic. Therefore, the bond dissociation enthalpy (BDE) of different An−H species can be considered as the main parameter that governs this mechanism. BDEs are calculated using the following formula (Eq. (2)):

$$BDE = H(An^{\bullet}, 298\,K) + H(H^{\bullet}, 298\,K) - H(An{-}H, 298\,K), \quad (2)$$

where H is for enthalpy, which takes into consideration temperature-dependent corrections [zero point energy (ZPE), translational, rotational and vibrational energies at 298 K]; H (An−H, 298 K) and H ($An^{\bullet}$, 298 K) are the enthalpies of the antioxidant (An−H) and its corresponding radicals ($An^{\bullet}$) obtained after the homolytic bond dissociation of An−H bond, respectively. H ($H^{\bullet}$, 298 K) is the enthalpy of hydrogen radical. BDE is an intrinsic parameter that helps to estimate the capacity of an antioxidant to release a hydrogen atom. The lower the BDE, the easier is the bond dissociation and the more important is the antioxidant activity. The ionization potential energies (IP) were calculated based on orbital consideration, which is based on Koopman's theorem where $IP = -E_{HOMO}$ [32].

The B3B86 hybrid functional proved as a reliable choice for the structure-antioxidant activity of antioxidant compounds and is deemed particularly adapted for BDE estimation by giving a high accuracy compared to the experimental value [25,33]. Herein, we extended the use of B3P86 to the series of compounds **1–10**. Previously, we tested the basis set effect on BDEs of hispidin and isohispidin isomers by using different basis sets, and the obtained BDEs showed differences lower than 0.4 kcal/mol for the active sites [11]. Consequently, for better accuracy, a triple basis set 6-311 + + G(d,p) is used. Hence, the geometry optimization of reactants and products of eq.1 were performed at the B3P86/6-6-311 + + G(d,p) level of theory. The minima were confirmed by vibrational frequency calculations (*i.e.*, no imaginary frequency). The solvent effects were taken into account implicitly by using the polarizable continuum model (PCM). In PCM, the substrate is embedded into a cavity surrounded by a dielectric continuum characterized by its dielectric constant (ε_{MeOH} = 32.613). The effect of aprotic solvent on BDEs values was considered by considering the dimethylsulfoxide solvent (DMSO). Different PCM formalisms are available. Here, the calculations were performed using the integral equation formalism variant (IEF-PCM) as implemented in the Gaussian09 program [34]. Trouillas et al., used a hybrid model (*i.e.*, one or two water molecules surrounding the active site of An−H + PCM) for natural quercetin, and they reported that obtained BDEs by considering the tested hybrid model were slightly different from those obtained within PCM [35]. Kosinova et al., have been tested the influence of different solvents including benzene, chloroform, ethanol, methanol, and water on BDEs values and compared to the experimental BDE obtained in benzene, and they conclude that the solvent influence was appeared to be weak, even by using a very polar dielectric constant like water [25] (Ref Pavlina). Herein, the effect of an aprotic solvent on BDEs values was considered by calculating BDEs values of **1** in PCM by using dimethyl sulfoxide as aprotic solvent (ε_{dmso} = 46.826).

All quantum calculations have been performed using DFT methods as implemented in Gaussian09 [34]. Electronic spin density delocalization of $An^{\bullet}$ was visualized using the Molden software (http://www.cmbi.ru.nl/molden/).

4.4.3. Molecular dynamics simulation

The primary protein-ligand complex file was prepared using DESMOND system builder panel which is inbuilt in the Schrödinger suite. Here all the protein-ligand complex systems were prepared periodic precondition with 10 $Å^3$ cubic boxes from the middle of mass with supermolecule. TIP3P water solvation system was used buffer system with charged ions placed isotopically to neutralize the Ewald charge

summation of the solvated protein entity. The system was minimized with maximum iterations of 5000 steps with a gradient convergence threshold of 1.0 kcal mol^{-1} $Å^{-1}$. Once the system is minimized the system is subjected to Newtonian dynamics of the model system to evaluate the energy of the system. 2ps steps were integrated to record the simulation. Six stages NPT ensemble default relaxation process were carried out before performing molecular dynamics simulation. Initially at first state solute restrained Brownian dynamics of ensemble was carried by keeping the energy constant using NVT condition. In the second stage using Berendsen thermostat the NVT (*canonical)* ensemble was allowed to relax with respect to temperature with velocity resembling of every 1ps applied to the non-hydrogen solute sample. Subsequently, NVT ensemble was changed to NPT ensemble with Berendsenbarostat with the system kept at 1 atm pressure followed by system equilibration of 1 ns. Then the ensemble was subjected to 20 ns Molecular dynamics run [36].

Acknowledgments

The publication was prepared with the support of the "RUDN University Program 5-100".The support of NSF-MRI Grant #1228232 for the purchase of the diffractometer and Tulane University for support of the Tulane Crystallography Laboratory are gratefully acknowledged.

Appendix A. Supplementary material

Supplementary data to this article can be found online at https://doi.org/10.1016/j.bioorg.2019.103193.

References

[1] A.R. Prasad, T. Ramalingam, A.B. Rao, P.V. Diwan, P.B. Sattur, Eur. J. Med. Chem. 24 (1989) 199–201.
[2] A.H. El-Masry, H. Fahmy, S. Ali Abdelwahed, Molecules 5 (2000) 1429–1438.
[3] A. Orabi, M. Moneim, E.E.-D. Salem, M.E.-D.A. El-Fattah, Polish J. Chem. 74 (2000) 1675–1683.
[4] T. George, D. Mehta, R. Tahilramani, J. David, P. Talwalker, J. Med. Chem. 14 (1971) 335–338.
[5] S. Buscemi, N. Vivona, T. Caronna, J. Org. Chem. 61 (1996) 8397–8401.
[6] B.R. Yoo, M.Y. Suk, Y.-M. Yu, S.G. Hong, I.N. Jung, Bull. Korean Chem. Soc. 19 (1998) 358–362.
[7] K. Paulvannan, T. Chen, R. Hale, Tetrahedron 56 (2000) 8071–8076.
[8] D. Catarzi, V. Colotta, F. Varano, L. Cecchi, G. Filacchioni, A. Galli, C. Costagli, V. Carlà, J. Med. Chem. 43 (2000) 3824–3826.
[9] Y. Ünver, S. Deniz, F. Celik, Z. Akar, M. Küçük, K. Sancak, J. Enzyme Inhib. Med. Chem. 31 (2016) 89–95.
[10] M. Chand, R. Kaushik, S.C. Jain, Turk. J. Chem. 42 (2018) 1663–1677.
[11] E.H. Anouar, S.A.A. Shah, N.B. Hassan, N.E. Moussaoui, R. Ahmad, M. Zulkefeli, J.-F.F. Weber, Molecules 19 (2014) 3489–3507.
[12] R. Al-Salahi, E.-H. Anouar, M. Marzouk, H.A. Taie, H.A. Abuelizz, Future Med. Chem. 10 (2018) 379–390.
[13] Y. El Bakri, E.H. Anouar, I. Marmouzi, K. Sayah, Y. Ramli, M. El Abbes Faouzi, E.M. Essassi, J.T. Mague, J. Mol. Model. 24 (2018) 179.
[14] Y. El Bakri, L. Guo, E.H. Anouar, A. Harmaoui, A.B. Ali, E.M. Essassi, J.T. Mague, J. Mol. Struct. 1176 (2019) 290–297.
[15] D. Chikazu, M. Shindo, T. Iwasaka, M. Katagiri, N. Manabe, T. Takato, K. Nakamura, H. Kawaguchi, J. Bone Miner. Res. 15 (2000) 674–682.
[16] M. Gupta, S. Paul, R. Gupta, Eur. J. Med. Chem. 46 (2011) 631–635.
[17] P. Sewell, F. Hawking, Brit. J. Pharmacol. 5 (1950) 239–260.
[18] R. Acheson, N. Taylor, J. Chem. Soc. (1956) 4727–4731.
[19] E. Essassi, J.P. Lavergne, P. Viallefont, J. Heterocycl. Chem. 13 (1976) 885–887.
[20] E. Essassi, J.-P. Lavergne, P. Viallffont, Tetrahedron 33 (1977) 2807–2812.
[21] M. Gupta, J. Heterocycl. Chem. 44 (2007) 1023–1027.
[22] K. Ajish, N. Joseph, M.P. Rani, K. Raghu, V. Vineetha, K. Radhakrishnan, Tetrahedron Lett. 54 (2013) 5682–5685.
[23] S. Karthikeyan, G. Bharanidharan, S. Ragavan, S. Kandasamy, S. Chinnathambi, K. Udayakumar, R. Mangaiyarkarasi, R. Suganya, P. Aruna, S. Ganesan, Mol. Pharm. 16 (2019) 669–681.
[24] S. Karthikeyan, G. Bharanidharan, S. Ragavan, S. Kandasamy, S. Chinnathambi, K. Udayakumar, R. Mangaiyarkarasi, A. Sundaramoorthy, P. Aruna, S. Ganesan, J. Chem. Inf. Model. 59 (2018) 326–338.
[25] P. Košinová, F. Di Meo, E.H. Anouar, J.L. Duroux, P. Trouillas, Int. J. Quantum Chem. 111 (2011) 1131–1142.
[26] G.M. Morris, R. Huey, W. Lindstrom, M.F. Sanner, R.K. Belew, D.S. Goodsell, A.J. Olson, J. Comput. Chem. 30 (2009) 2785–2791.
[27] X. Shen, W. Saburi, Z. Gai, K. Kato, T. Ojima-Kato, J. Yu, K. Komoda, Y. Kido, H. Matsui, H. Mori, Acta Crystallogr. D 71 (2015) 1382–1391.
[28] S. Caner, X. Zhang, J. Jiang, H.M. Chen, N.T. Nguyen, H. Overkleeft, G.D. Brayer, S.G. Withers, FEBS Lett. 590 (2016) 1143–1151.
[29] E. Anouar, C. Calliste, P. Kosinova, F. Di Meo, J. Duroux, Y. Champavier, K. Marakchi, P. Trouillas, J. Phys. Chem. A 113 (2009) 13881–13891.
[30] J.M. Mayer, D.A. Hrovat, J.L. Thomas, W.T. Borden, J. Am. Chem. Soc. 124 (2002) 11142–11147.
[31] O. Tishchenko, D.G. Truhlar, A. Ceulemans, M.T. Nguyen, J. Am. Chem. Soc. 130 (2008) 7000–7010.
[32] T. Koopmans, Physica 1 (1934) 104–113.
[33] P. Trouillas, P. Marsal, D. Siri, R. Lazzaroni, J.-L. Duroux, Food Chem. 97 (2006) 679–688.
[34] M. Frisch, G. Trucks, H. Schlegel, G. Scuseria, M. Robb, J. Cheeseman, G. Scalmani, V. Barone, B. Mennucci, G. Petersson, Gaussian 09, revision D. 01, Gaussian, Inc., Wallingford CT, 2009.
[35] D. Kozlowski, P. Trouillas, C. Calliste, P. Marsal, R. Lazzaroni, J.-L. Duroux, J. Phys. Chem. A 111 (2007) 1138–1145.
[36] K.J. Bowers, D.E. Chow, H. Xu, R.O. Dror, M.P. Eastwood, B.A. Gregersen, J.L. Klepeis, I. Kolossvary, M.A. Moraes, F.D. Sacerdoti, Scalable algorithms for molecular dynamics simulations on commodity clusters, SC'06: Proceedings of the 2006 ACM/IEEE Conference on Supercomputing, IEEE, 2006, pp. 43–43.